Arteries and Algorithms: Multiple scale modelling of flow in the Cardiovascular system

Spencer Sherwin[1], Jordi Alastruey[1,2], Andrew Cookson[1], Denis Doorly[1], Asimina Kazakidi[1,2], Kim Parker[2], Joaquim Peiro[1], Peter Weinberg[2]

[1]*Bioflow Group, Department of Aeronautics, Imperial College London*
London, SW7 2AZ, UK
[2]*Department of Bioengineering, Imperial College London*
London, SW7 2AZ, UK

Email: *s.sherwin@imperial.ac.uk*

ABSTRACT

This review outlines some of the different scales involved in computationally modelling arterial networks. Starting at the largest O(1m) scale we highlight current activities in reduced modelling of the pulse waves. We then focus on the O(10^{-1}m) scale and provide an example of how CFD can be applied to understand the role of mixing in small amplitude helical pipes at physiologically relevant flow conditions. Finally we motivate the interaction at O(10^{-3}m) scale by considering how localised flow features are suggestive of different types of arterial disease patterns.

1. OVERVIEW

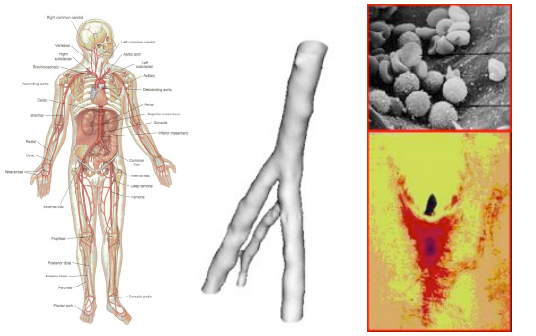

Arterial tree *O(1)* | Vessel branching *O(10^{-1})* | Localized disease *O(10^{-3})*

Figure 1: The largest flow related scales of the cardiovascular system

Flow in the arterial networks exerts numerous effects on the vessels by virtue of the stresses it imposes on them and the mass and heat it transports. The biological and mechanical interactions in the vessels involve complex multi-scale coupling between fluid dynamics, vascular mechanics and vascular biology. For example, as shown in the figure 1, the pulse waves observed in the different arteries are influenced by the O(1) scale of the network topology through wave reflections. The wave patterns then influence the non-linear flow features at the O(10^{-1}) scale of the arterial branches. The blood flow at branches is widely accepted to be related to the formation of arterial plaques involving the O(10^{-3}) scale of the blood particles and vessel cells. An even longer cascade of scales can then be considered from the cellular scale right down to the genomic level.

In this review we will start in section 2 by the pulse wave modelling of flow in the cardiovascular system dating back to the work of Euler in 1775 [1]. A series of subsequent mathematical developments, including computational modelling techniques, have allowed for a complete solution of the wave propagation in the larger arterial vessels to be obtained. After outlining the current state of the art modelling of pulse wave propagation, in section 2, we discuss how mechanics based, computational modelling can also simulate the complex flow patterns that arise in the localised arterial geometries which are associated with the progression of disease. Therefore in section 3 we introduce the problem of mixing in small amplitude pipes relevant to the design of bypass grafts and potentially a natural feature of many physiological vessels. Finally in section 4 we will discuss how localised flow features are indicative of aspects of the arterial disease patterns.

2. REDUCED MODELLING OF PULSE WAVE PROPAGATION IN THE CARDIOVASCULAR SYSTEM: VALIDATION AND APPLICATIONS

Pulse waveforms in the cardiovascular system are useful as a diagnostic tool in clinical practice because they carry information about the morphology and functionality of the system. A good understanding of the mechanics of pulse wave propagation under normal conditions and the impact of disease and anatomical variations on the propagation patterns will provide valuable information for clinical diagnosis and treatment of cardiovascular diseases whose initiation and progression depend on haemodynamic quantities such as blood pressure, blood flow and wall shear stress. Although there is a growing interest in three-dimensional (3-D) simulations, the one-dimensional (1-D) equations of blood flow in compliant vessels offer a good compromise between accuracy and computational cost when a global assessment of the arterial system is required, since arterial pulse wavelengths are about three orders of magnitude larger than arterial diameters in normal conditions. Reduced modelling is also useful to provide the boundary conditions for 3-D simulations.

We have developed an algorithm to solve the nonlinear, 1-D equations in arterial networks using a discontinuous Galerkin scheme with a spectral/*hp* spatial discretisation [14,13,3] in which several lumped parameter, or zero-dimensional (0-D), models of the perfusion of the microcirculation can be coupled in the time domain [9]. The 1-D discontinuous Galerkin algorithm was initially validated by comparison against a Taylor-Galerkin formulation [13]. The 1-D equations were successfully tested in [3] against measurements in the aorta of an experimental 1:1 latex replica of the left heart and the human arterial tree [12]. An additional test of the 1-D equations was presented in [12] by comparing experimental and numerical pressures and flows in an improved *in vitro* 1:1 replica of the systemic circulation (Figure 2), in which the parameters required by the numerical model were directly measured and no data fitting was involved. Average relative root-mean-square errors between simulations and experimental waveforms were smaller than 4% for pressure and 19% for the flow at all 70 locations studied. The same relative errors were obtained using the linear formulations, suggesting that the effect of nonlinearities on pulse waveforms is only secondary.

The 1-D/0-D model was initially applied to study blood flow in arterial placental networks in a monochorionic twin pregnancy with an arterio-arterial anastomosis and an arterio-venous

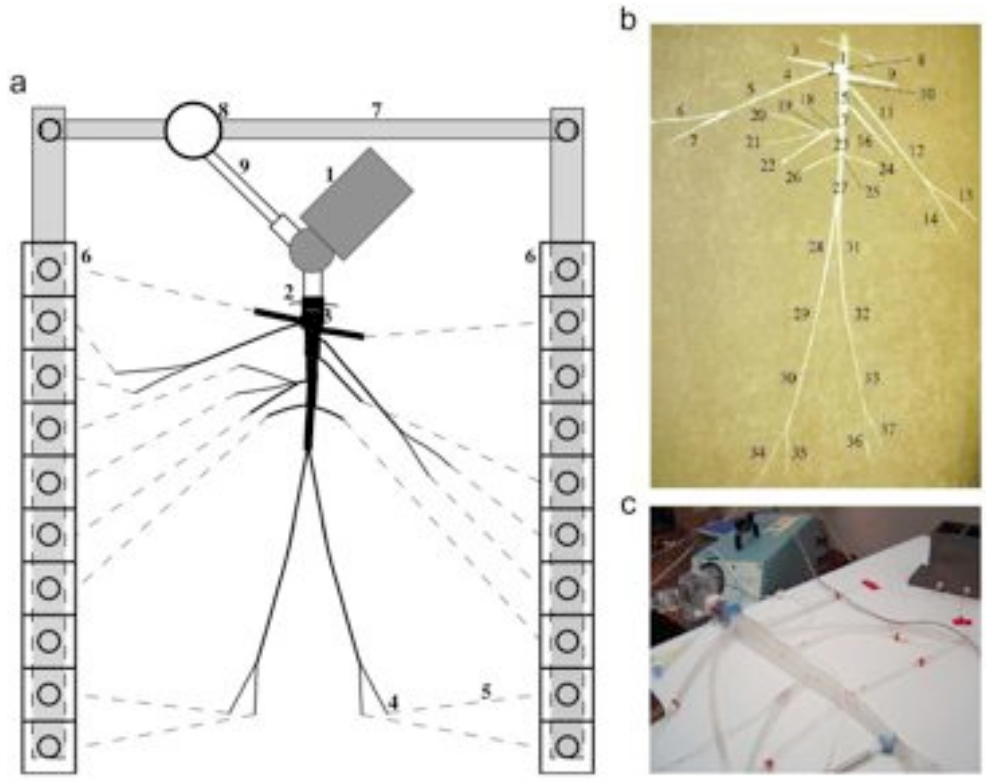

Figure 2: (a) Planview schematic of the in vitro model simulating the left heart and the largest 37 conduit systemic arteries in the human. 1: Pump (left heart); 2: catheter access; 3: two-leaflet aortic valve; 4: peripheral resistance tube; 5: stiff plastic tubing (veins); 6: venous overflow; 7: venous return conduit; 8: buffering reservoir; 9: pulmonary veins. (b) The 37 arteries simulated. (c) Detail of the pump and the aorta. (Taken from [11]).

anastomosis [10]. This study focused on the effects of the time period of the two fetus' heartbeats and the role of terminal resistance in the network. Our next models benefited from the algorithm proposed in [9] to estimate peripheral resistances and compliances from *in vivo* data. The effect of cross-connections between arteries on pulse waveforms were studied in arm and cerebral networks. The arm model [7] was applied to assess the reliability of the modified Allen's test, a clinical technique to detect the presence of sufficient collateral flow through the palmar arch arteries if radial blood supply is interrupted (e.g., when the radial artery is harvested and used as a coronary artery bypass graft). This study showed that small calibres in the collateral arteries or insufficient compression of the radial artery could lead to false-positive results, and proposed a more reliable alternative technique. The cerebral model [6] was applied to study the compensatory ability of the most frequent anatomical variations of the circle of Willis (CoW) (a ring-like arterial network located at the base of the brain), in normal conditions and after occlusion of an inflow (carotid or vertebral) artery. This study identified the critical collateral pathways of the CoW and showed that cerebral pulse waveforms provide valuable information on the anatomy of the CoW. These findings are important to understand the factors that increase the risk of insufficient blood supply to the brain during surgical procedures in the inflow arteries of the CoW, such as carotid endarterectomy (surgical incision to remove plaque in patients with a severe carotid occlusion). The cerebral model was coupled to a lumped parameter model of metabolic flow auto-regulation [4], which allowed a better understanding of the risk factors previously discussed in [6]. More recently, the 1-D model was applied to simulate the rabbit systemic circulation in order to interpret changes in pulse waveform observed *in vivo* after administering drugs that alter nitric oxide synthesis [5]. This model allowed us to test hypotheses that cannot be addressed *in vivo* for technical and physiological reasons and to elucidate the haemodynamic mechanisms underlying previously observed changes in pulse waveforms produced *in vivo* by vasoactive drugs. According to the model, these changes can be explained by single or combined alterations of blood viscosity, peripheral resistance and compliance.

The 1-D model was also very useful for understanding the mechanics behind the main features observed in vivo in Arterial pulse waveforms [3,2,7]. The applicability of the algorithms proposed in [2,8] to separate the reservoir and wave components of pulse waveforms was tested using numerical data obtained with the 1-D model. Our current research on reduced blood flow modelling focuses on the development of an algorithm to systematically follow the waves generated by a single wavefront propagating from the root of an arterial network, which will allow us to analyse the pattern of pulse waves and their relation to the reflection points in the network [8].

3. Mixing of Steady Flow in Small Amplitude Helical Pipes For Medical Applications.

More than 500,000 coronary artery bypass grafts are fitted each year worldwide. However, over 50% of these fail within 10 years, due to thrombosis and neo-intimal hyperplasia. Small amplitude helical pipes have been proposed for use as arterio-venous shunts and bypass grafts [15]. Preliminary *in vivo* tests found that conventional grafts were completely occluded by thrombosis, whereas grafts constructed with helical pipes were not. Swirling flow and in-plane mixing induced by the geometry were hypothesised to be the mechanisms responsible. This work investigates numerically the mixing behaviour of steady flow in helical geometries, typical of those for use in medical applications [16].

3.1 Methods

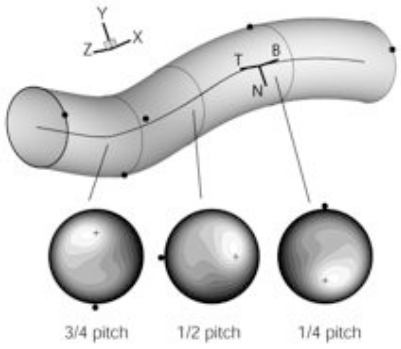

Figure 3: Typical helical pipe geometry, *R=0.25D,* for use in medical applications. The self-similar velocity field, shown by the contour plots of axial velocity, rotates along the pipe.

A helix is a 3-dimensional space curve, which can be described by the following equations:

$$x = R\cos(z/c),\ y = R\sin(z/c)$$

where R is the radius or amplitude of the helix, and c is a parameter such that one pitch length of the helix is $2\pi c$. Helical pipes of small amplitude, as in Figure 3, can be reasonably approximated as a circular

cross-section translated by a helical centreline. Using this approximation, the flow is solved with a coordinate mapping, which allows the Navier-Stokes equations, plus an additional body-force term, to be solved within a cylindrical geometry. This is accomplished using a finite-element formulation on the cross-sectional mesh, and a Fourier basis function in the periodic, z coordinate [16,17].

The helical pitch length was fixed at 6 pipe diameters (D), and the helical radius (R) varied from $0.1D$ to $0.5D$. A physiologically appropriate Reynolds number of 250 was used for all cases. Mixing is the process of advection and diffusion [18], although for the haemodynamic species of interest, diffusion is negligible. Therefore only advection is examined, by tracking the uniform grid of passive particles shown in Figure 4(a), for several helical pitch lengths.

3.2 Results

The velocity field in a helical pipe is self-similar along the centreline, performing a rotation of 2π over one pitch length, as shown by the axial velocity contour plots in Figure 3. As the helical radius, R, is increased, the axial velocity profile becomes more asymmetric, and the peak value of velocity moves towards the wall. The secondary flow is dominated by a single vortical structure for all the cases considered. The strength of this vortex, shown for $R=0.25D$ in Figure 5(f), increases with R.

3.2.1 Particle trajectories

Figures 4(b-f) show slices of the particle trajectories after five helical pitch length, $z=30D$, for the cases $R=0.1D$ to $0.5D$, in increments of $0.1D$. Despite the secondary flow being a single vortical structure, a double-vortex pattern, similar to that of Dean flow, clearly emerges in the particle trajectories as R is increased. This apparent discrepancy was first reported in the computational and smoke visualisation results of Yamamoto *et al.* [19]. We show that it can be explained using a sequence of coordinate transformations or changes in reference frame.

The cross-sectional plane, by definition, undergoes translation along the helix, and as Figure 3 shows, the velocity field undergoes rotation. The movement of the particles within the plane can be explained by removing both of these motions:

$$\boldsymbol{V}_{in\text{-}plane} = \boldsymbol{V}_{cartesian} - \boldsymbol{V}_{translation} - \boldsymbol{V}_{rotation}$$

Figure 5(b) shows that the streamtraces for the cross-sectional flow in the Cartesian reference frame are not constrained within the boundary. This is due to the movement of the plane along the helix, and hence the streamtraces are sensible in the context of the *3-D* geometry. Subtracting $\boldsymbol{V}_{translation}$, to remove the effects of this motion, produces the streamtraces in Figure 5(c). These are now constrained with the plane, and correspond approximately to the vortical structure in the flow, Figure 5(f). The streamtraces of $\boldsymbol{V}_{rotation}$ are shown in Figure 5(d). The magnitude is proportional to the axial velocity, and hence the maximum velocity corresponds spatially to the peak axial velocity. Subtracting this rotation gives $\boldsymbol{V}_{in\text{-}plane}$, the streamtraces and magnitude of which are shown in Figure 5(e).

The emergence of the double vortex structure can be explained by examining the magnitude and distribution of each of the velocity components as they vary with R. For all the geometries the circulation of the vortex $\boldsymbol{V}_{rotation}$ is the same. However as R is increased, the location of the peak velocity moves towards the wall, and away from the peak velocity of the vortical structure. For $R=0.1D$ the vortical structure is very weak compared to $\boldsymbol{V}_{rotation}$, and $\boldsymbol{V}_{in\text{-}plane}$ is therefore the single vortex shown in

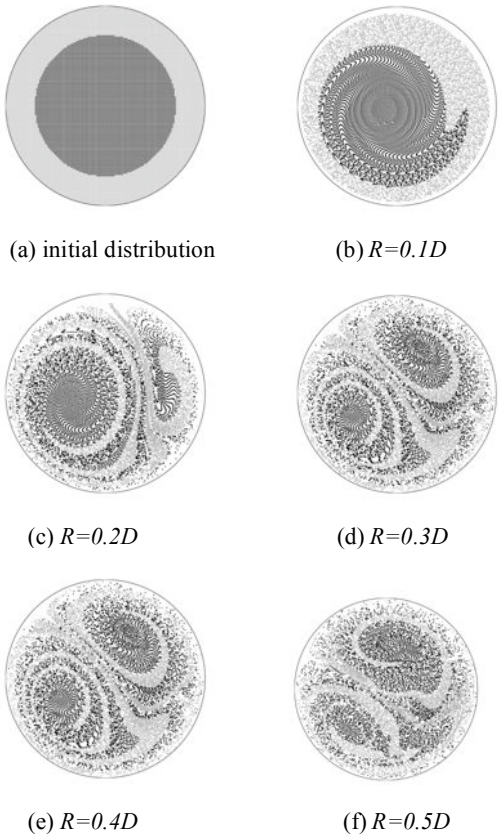

(a) initial distribution (b) $R=0.1D$

(c) $R=0.2D$ (d) $R=0.3D$

(e) $R=0.4D$ (f) $R=0.5D$

Figure 4: Particle trajectory slices at z=30D (five pitches) for varying helical radius

Figure 5(b). As R increases, the strength of the vortical structure increases, which combined with the offset of the peak velocity, means that the size of the second vortex existing in $\boldsymbol{V}_{in\text{-}plane}$ also increases.

3.2.2 Quantification of mixing, and its relationship with geometry

Figures 4(b-f) show a qualitative increase in mixing with increasing R, caused by the emergence of the double-vortex structure in the in-plane flow. The degree of mixing increases with downstream distance [16].

Conceptually, mixing is the reduction of non-uniformity, or equivalently, the increase of disorder. Information entropy was first defined by Shannon [20], and can be interpreted as a measure of disorder. A formulation introduced to study chaotic micromixers [21] is used here. In [21] passive, coloured particles were tracked through the micromixer, taking sections of the trajectories at areas of interest. A grid was superimposed onto the section, and Equation (1) applied.

$$S = \sum_{i=1}^{N_c}\left[w_i \sum_{k=1}^{N_s} \left(n_{i,k} \log n_{i,k} \right) \right] \tag{1}$$

In Equation (2), i is the cell index, k is the species index, w *is* the weighting factor for each cell, N the number of cells, N the number of species (i.e. different colours of particles) and $n_{i,k}$ is the particle number fraction of the k^{th} species in the i^{th} cell. The weighting factor w_i is defined so that it is zero if a cell contains no particles, or only particles of a single species/colour; within such a cell the particle distribution is uniform, and therefore should contribute zero to the entropy summation, i.e. disorder can only occur if particles of different colours are present. As Figure 4 shows, only two colours of particles are used throughout this work.

As a value considered in isolation, the entropy calculated in (1) has little meaning. Again following Kang and Kwon we define a relative entropy measure κ, which quantifies the increase in entropy of the particle distribution at a particular cross-section from that of the inlet distribution of particles. This is then normalised by the maximum possible entropy increase from the inlet particle distribution, and is defined as

$$\kappa = \frac{S - S_0}{S_{\max} - S_0} \tag{2}$$

From the above it can be appreciated that when κ is equal to zero, no mixing has occurred, and when κ equals one, the mixing is maximised. Figure 6 shows

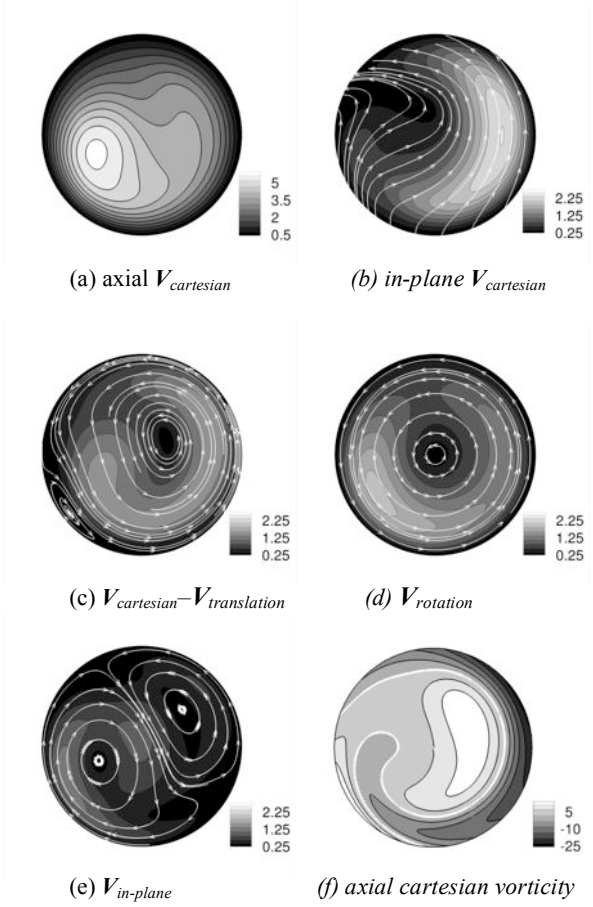

(a) axial $\boldsymbol{V}_{cartesian}$ *(b) in-plane* $\boldsymbol{V}_{cartesian}$

(c) $\boldsymbol{V}_{cartesian}$–$\boldsymbol{V}_{translation}$ *(d)* $\boldsymbol{V}_{rotation}$

(e) $\boldsymbol{V}_{in\text{-}plane}$ *(f) axial cartesian vorticity*

Figure 5: In-plane velocity transformations to obtain particle trajectories

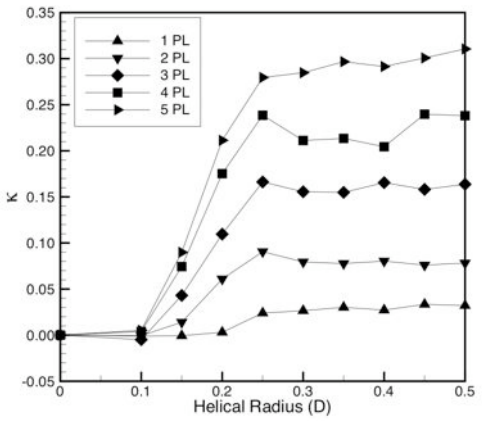

Figure 5: Relative entropy increase, κ for increasing helical radius - calculated at integer multiples of the pitch length

κ plotted against increasing helical radius, for integer multiples of the pitch length. It is clear that κ increases sharply with *R* up to *R=0.25D*, but very little beyond this. This is due to the double-vortex structure only changing slightly for *R > 0.25D*.

3.3 Summary

The results presented here both quantify and explain the variation of mixing with helical radius, showing that mixing increases sharply up to *R=0.25D* but little beyond. In [16] we show that the pressure drop over one pitch length of the helix increases approximately linearly with *R* suggesting that if mixing, as quantified here, is beneficial for medical applications, a geometry with *R=0.25D* will provide these benefits, whilst minimising physiologically costly pressure losses.

4. COMPUTATIONAL MODELLING OF BLOOD FLOW IN THE THORACIC AORTA: RELATION TO ATHEROSCLEROTIC LESION LOCATIONS

Blood flow in the thoracic aorta near side branches is computed using high-order unstructured spectral/hp element methods [17]. The objective is to study the role of different haemodynamic parameters in the localization of atherosclerosis, a disease that is responsible for the majority of myocardial infarctions and which is prevalent in Western societies. The patchy distribution of atherosclerosis in regions of haemodynamic stresses exerting a controlling influence on its rate of development. The current consensus is that lesions occur most frequently in regions of low and fluctuating haemodynamic wall shear stress. However, patterns of lesion prevalence around the origins of intercostal arteries in the descending thoracic aorta are known to vary with age and species [22]. We test the hypothesis that these variations could reflect differences in the pattern of shear stress exerted on the wall by the flow of blood.

The emergence of an intercostal artery from the dorsal wall of the descending thoracic aorta, which has a 10-fold larger diameter, is modelled as a cylindrical tube emerging perpendicularly from a flat plate (figure 6a) [23,24]; the idealised geometry simplifies interpretation of effects of the Reynolds number and side branch flow rate. Using the Newtonian incompressible Navier-Stokes equations, high-order steady and pulsatile flow computations are performed and flow and wall shear stress (wss) patterns are analysed. Reversing and non-reversing side branch flows are examined [25]. In addition, the study is extended to examine flows in more realistic geometries, such as different configurations of pairs of intercostal arteries, geometries approximating those seen in histological sections and corrosion casts, and anatomically correct models reconstructed from micro-CT images of corrosion casts of rabbit aortas made at physiological pressure.

This study shows that patterns of flow and wss are strikingly dependent on haemodynamic conditions.

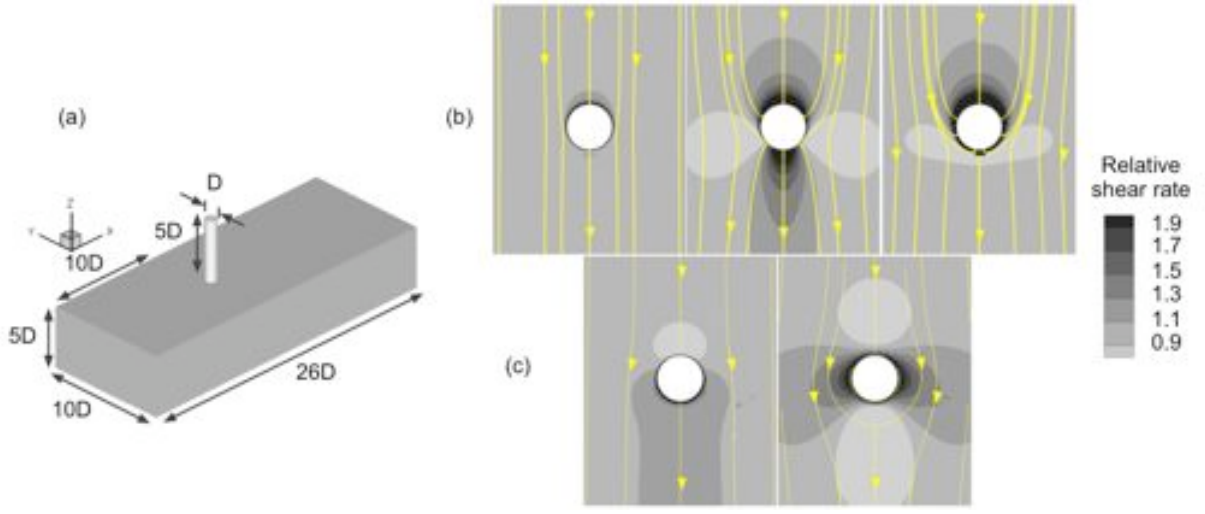

Figure 6: (a) Model of intercostal artery. (b) Wall shear stress maps under steady flow conditions. (c) Wall shear stress maps for reversing side branch flow rate.

arterial curvature and branching is consistent with

Varying the Reynolds number and the side branch

flow rate, either independently or in combination, alters the wss distribution in steady flow (figure 6(b)). With increasing Reynolds number, stresses are lowered at the sides of the branch ostium and increased upstream and downstream. Increased flow into the side branch enlarges the areas where shear is altered and intensifies the differences in its magnitude. It also moves the low-shear side lobes and stagnation region downstream. Under unsteady flow conditions and for non-reversing side branch flow, the effect of pulsatility is small. However, significantly different wss patterns are generated when the side branch flow is made to reverse for part of the cycle (figure 16c). Arterial geometrical features appear to have little influence on the wall shear stress pattern. Aspects of the patterns observed in this study correlate well with, and may explain, lesion patterns seen in human, rabbit and mouse aortas.

REFERENCES

[1] L. Euler, Principia pro motu sanguinis per arterias determinando. Opera posthima mathematica et physica anno 1844 detecta, 2 (1775) 814–823. ediderunt PH Fuss et N Fuss Petropoli; Apund Eggers et Socios.

[2] J. Aguado-Sierra, J. Alastruey, J.J. Wang, N. Hadjiloizou, J.E. Davies, and K.H. Parker. Separation of the reservoir and wave pressure and velocity from measurements at an arbitrary location in arteries. *Accepted to Proc. Inst. Mech. Eng., Part H*, J. Eng. Med., 2008.

[3] J. Alastruey. Numerical modelling of pulse wave propagation in the cardiovascular system: development, validation and clinical applications. *Ph.D. thesis, Imperial College London, University of London,* 2006.

[4] J. Alastruey, S.M. Moore, K.H. Parker, T. David, J. Peiro, and S.J. Sherwin. Reduced modelling of blood flow in the cerebral circulation: Coupling 1-D, 0-D and cerebral auto-regulation models. *Int. J.Num. Meth. Fluids*, 56:1061–1067, 2008.

[5] J. Alastruey, S.R. Nagel, B.A. Nier, A.A.E. Hunt, P.D. Weinberg, and J. Peiro. Modelling pulse wave propagation in the rabbit systemic circulation to assess the effects of altered nitric oxide synthesis. *Submitted to Hypertension,* 2008.

[6] J. Alastruey, K.H. Parker, J. Peiro, S.M. Byrd, and S.J. Sherwin. Modelling the circle of Willis to assess the effects of anatomical variations and occlusions on cerebral flows. *J. Biomech*., 40:1794–1805, 2007.

[7] J. Alastruey, K.H. Parker, J. Peiro, and S.J. Sherwin. Can the modified Allen's test always detect sufficient collateral flow in the hand? A computational study. *Comp. Meths. Biomech. Biomed. Eng*., 9:353–361, 2006.

[8] J. Alastruey, K.H. Parker, J. Peiro, and S.J. Sherwin. Analysing the pattern of pulse waves in arterial networks. *Submitted to J. Eng. Maths*., 2008.

[9] J. Alastruey, K.H. Parker, J. Peiro, and S.J. Sherwin. Lumped parameter outflow models for 1-D blood flow simulations: Effect on pulse waves and parameter estimation. *Comm.. Comput. Phys*., 4:317–336, 2008.

[10] V.E. Franke, K.H. Parker, L.Y. Wee, N.M. Fisk, and S.J. Sherwin. Time domain computational modelling of 1D arterial networks in monochorionic placentas. *Mathem. Mod. and Num. Analysis*, 37:557–580, 2003.

[11] K.S. Matthys, J. Alastruey, J. Peiro, A.W. Khir, P. Segers, P.R. Verdonck, K.H. Parker, and S.J.Sherwin. Pulse wave propagation in a model human arterial network: Assessment of 1-D numerical simulations against in vitro measurements. *J. Biomech*., 40:3476–3486, 2007.

[12] P. Segers, F. Dubois, D. De Wachter, and P. Verdonck. Role and relevancy of a cardiovascular simulator. *Cardiov. Eng*., 3:48–56, 1998.

[13] S.J. Sherwin, L. Formaggia, J. Peiro, & V.E. Franke. Computational modelling of 1D blood flow with variable mechanical properties and its application to the simulation of wave propagation in the human arterial system. *Int. J. Num. Meth. Fluids,* 43:673–700, 2003.

[14] S.J. Sherwin, V.E. Franke, J. Peiro, and K.H. Parker. One-dimensional modelling of a vascular network in space-time variables. *J. Eng. Maths*., 47:217–250, 2003.

[15] C.G. Caro, N.J. Cheshire, N. Watkins, Preliminary comparative study of small amplitude helical and conventional eptfe arteriovenous shunts in pigs. *J. Roy. Soc. interface* 2, 261–266, 2005

[16] A.N. Cookson, D.J. Doorly, S.J. Sherwin, Mixing Through Stirring of Steady Flow in Small Amplitude Helical Pipes. *Annals of Biomedical Engineering, submitted*. 2008,

[17] S.J. Sherwin, G.E. Karnaidakis, 2005. Spectral/hp Element Methods for Computational Fluid Dynamics. *Oxford Science Publications*, 2005

[18] J.M. Ottino, The kinematics of mixing: stretching, chaos, and transport. *Cambridge University Press.* 1989

[19] K. Yamamoto, A. Aribowo, Y. Hayamizu, Hirose, T., Kawahara, K. Visualization of the flow in a helical pipe. *Fluid Dynamics Research* 30, 251–267, 2002.

[20] C.E. Shannon, A mathematical theory of communication. *Bell System Technical Journal* 27, 379–423. 1948

[21] T.G. Kang, T.H. Kwon, Colored particle tracking method for mixing analysis of chaotic micromixers. *Journal of Micro-mechanics and Microengineering* 14, 891. 2004.

[22] P. Weinberg, Disease Patterns at Arterial Branches and their Relation to Flow, *Biorheology,* 39, 533-537, 2002

[23] I. Sobey, "Laminar boundary-layer flow past a two-dimensional slot", *J. Fluid Mech*., 83, 33-47, 1977.

[24] O. Tutty, "Flow in a tube with a small side branch", *J. Fluid Mech*., 191, 79-109, 1988.

[25] G. Sloop, R. Perret, J. Brahney, M. Oalmann, A description of two morphologic patterns of aortic fatty streaks, and a hypothesis of their pathogenesis, *Atherosclerosis*, 141, 153-160, 1998